

Performance Modeling of Urban Air Mobility Vehicles to Support Air Traffic Management Research

David Hartman¹, John Foster²

NASA Langley Research Center, Hampton, Virginia 23681

Christopher Hartman³

Analytical Mechanics Associates, Inc., Hampton, VA 23666

The recent emergence of Urban Air Mobility (UAM) vehicles has resulted in a need for flight performance models that enable comprehensive simulation-based research on air traffic management topics such as route structure, scheduling, and separation standards. Successful performance modeling methods exist for a wide range of traditional aircraft designs. However, comparable modeling methods appropriate for UAM vehicles that combine fixed-wing and rotorcraft performance have not yet been established. One challenge to progress has been the lack of available data capturing the performance characteristics and unique flight profiles of these aircraft. This paper describes methods used to generate the required performance data and the development of performance models for UAM vehicles. Included is a review of the energy and power equations often used in developing performance models for traditional aircraft as well as a discussion of their applicability to UAM vehicles. The challenge of generating realistic performance data in over-actuated vehicles transitioning from hover to cruise flight is also addressed through an approach based on objective function optimization. A table-based performance model format adapted to UAM configurations is described, as well as parametric models intended to accompany the performance table to allow detailed modeling of power and fuel consumption during accelerated flight, turning flight, or flight at an arbitrary climb or descent rate. A discussion of future work is also provided, including the need for refinement of UAM performance modeling methods and formats, especially in conjunction with improvements to aerodynamic modeling of vehicles with complex designs where strong interaction effects may dominate important regions of the flight envelope.

I. Introduction

One of the challenges facing Air Traffic Management (ATM) researchers in Urban Air Mobility (UAM) is a lack of “performance models” that capture the unique characteristics of these aircraft, such as nominal airspeeds, climb rates, and flight paths. UAM vehicles are designed to support high-density operations in urban and suburban environments [1], often incorporating a diverse range of innovative design features to enable vertical take-off and landing (VTOL), increased efficiency, and quiet flight. Designs might include a combination of stoppable and stowable rotors, tiltrotors, and fixed and variable pitch propellers, in addition to aerodynamic lifting surfaces such as fixed or tilting wings. Specific examples analyzed in recent publications include specialized helicopter designs, multirotor, tiltrotor, and tiltwing aircraft, and lift plus cruise vehicles [2–4]. While many unique concepts have been proposed, the detailed data needed to generate realistic performance models is not widely available. The NASA Revolutionary Vertical Lift Technology (RVLT) project has published numerous conceptual vehicle designs based on the UAM mission described in Ref. [5], utilizing NASA Design and Analysis of Rotorcraft (NDARC) software [6] to size these vehicles [2–4] and incorporating certain baseline assumptions about vehicle technologies described in Ref. [7]. Among the available NASA designs are fully electric six-passenger quadrotor, “lift+cruise” (L+C), and tiltwing concepts with either fully electric or turboelectric hybrid powertrains. These concepts are valuable resources for understanding the unique characteristics of UAM vehicle performance and operations.

This paper describes the development of performance models for several UAM vehicles. The organization of the paper is as follows: Section II provides an overview of an existing performance modeling method for traditional fixed-wing and helicopter vehicles and considers the critical differences between these models and the unique characteristics

¹ Research Aerospace Engineer, Flight Dynamics Branch, Bldg. 1232/MS 308, david.c.hartman@nasa.gov

² Senior Research Engineer, Flight Dynamics Branch, Bldg. 1232/MS 308, john.v.foster@nasa.gov, AIAA Associate Fellow

³ Senior Aerospace Engineer, NASA LaRC, Bldg. 1209/MS 442, christopher.l.hartman@ama-inc.com

of UAM vehicle designs. Section III describes the NASA UAM vehicle designs that were modeled and details the methods used to obtain representative performance data for these aircraft. Section IV describes the analysis methods that were used, and the structure of the performance model adopted for this work. Finally, Section V serves as a conclusion and highlights areas for future work.

II. Overview of Performance Modeling Methods

Aircraft performance models are used in many areas of ATM systems analysis. Applications include airspace and procedure design, traffic separation, trajectory generation and prediction, real-time and fast-time simulations, and others [9,10]. Performance models are typically constructed with the aim of balancing competing objectives, which might include maximizing predictive accuracy while limiting model complexity. This balance might be achieved in part by making assumptions about the way the vehicle will be operated as well as by fitting the performance variations of the vehicle to a regression model with limited degrees of freedom and an assumed domain of applicability. Various types of performance models have been developed, and these are sometimes categorized based on their mathematical structure and degrees of freedom as point-mass models, kinematic models, kinetic models, and others not precisely fitting these categories [8]. Performance models often include details such as nominal airspeeds and climb or descent rates for various segments of flight as a function of weight and altitude, as well as fuel burn (or battery consumption) for typical operating conditions. Basic performance limitations of the aircraft are also commonly provided with the model, though the level of detail and format of these limitations can vary substantially. Notably, typical performance models do not explicitly address vehicle dynamics, and generally are not provided as stand-alone simulations. This means that performance characteristics which are substantially dependent on piloting or flight control system tuning, such as acceleration profiles, are typically not included and must be assumed by the user separately from the performance model. In this way, performance models are often coupled with software designed specifically to work in the intended application and to be compatible with the format of the performance model used.

Among the most ubiquitous performance models are those produced by EUROCONTROL as the Base of Aircraft Data (BADA), which are available under agreement. Several BADA model families have been developed, with each making specific mathematical assumptions about vehicle performance and having a specified file format. These include the BADA 3 [10] and more detailed BADA 4 [11] models, which are primarily focused on fixed-wing vehicles, and the BADA H [12] models intended to capture helicopter performance. While the BADA models have proven successful in serving their intended purposes, they were only designed for specific aircraft classes and therefore are not directly applicable in their present form to UAM vehicles or operations. One obstacle is that the parametric regression models used in BADA for fixed-wing and rotary-wing vehicles may not effectively capture the complex performance variations of UAM vehicles, which are often designed to combine rotary-wing flight at low-speed with fixed-wing performance at high speeds. While some preliminary work has explored model structures intended to address this problem (see e.g., Ref. [13]), the large variability in UAM vehicle design, coupled with the unique needs of UAM ATM research applications, has not yet led to the development of a widely accepted performance model structure for these aircraft. Nevertheless, the approach used for BADA models serves as a useful basis for development of UAM models and the following sections discuss important model features with a focus on the BADA 3.

A. Performance Model Format

BADA 3 performance models are composed of a collection of text files and are based on detailed documentation describing their use. These models cover a very large number of aircraft, with over three hundred types included in BADA 3 [10]. In the provided documentation, six types of files are described, four of which are relevant to this discussion. The “Operations Performance File (OPF)” and “Airline Procedure File (APF)” contain performance parameters and speed procedure parameters respectively for each aircraft type modeled. The parameters contained in the OPF and APF are used in conjunction with mathematical models and performance assumptions detailed in Ref. [10] to allow vehicle performance to be calculated in a manner suitable for many ATM trajectory simulation and prediction algorithms. The OPF and APF files are typically generated based on a modeling process that optimally fits the parametric degrees-of-freedom to available performance data. This performance data might be obtained from a combination of sources, including aircraft manufacturers, operators, pilots, air traffic controllers, and radar flight data [14]. Once the OPF and APF parameters are determined for the aircraft type, the “Performance Table File” (PTF) and “Performance Table Data” (PTD) files can be automatically generated based on the parameters in the OPF and APF files and the modeling assumptions inherent to BADA 3 [10]. A PTF and PTD file for each aircraft type is provided, and these contain convenient tabular data summarizing the performance of the aircraft in a format that is easy to read. The performance data includes fuel burn rate, airspeed, and climb or descent rate as a function of altitude, payload,

and flight segment. The difference between the PTF and PTD files is primarily the level of detail contained in each. The PTD contains additional intermediate calculation values but is otherwise comparable to the PTF.

B. The Total Energy Model

The ‘‘Total Energy Model’’ (TEM) is a commonly used mathematical approach to modeling flight path performance and is a fundamental feature of BADA models. The general form of the TEM described in Ref. [10] (see also Refs. [13,14]) can be derived by assuming a point-mass model of the vehicle and considering the change in the potential and kinetic energy of the aircraft due to thrust and drag forces acting on the vehicle. To illustrate, consider the sum of the potential and kinetic energy of a point-mass model of the vehicle to be its mechanical energy (E_{mech}) as given by Eq. (1), where m is the vehicle mass, g_0 is the acceleration due to gravity, h is the geodetic altitude, and V_{TAS} is the true airspeed.

$$E_{mech} = mg_0h + \frac{1}{2}mV_{TAS}^2 \quad (1)$$

Note that this model omits energy associated with rotating components, such as the vehicle’s rotors. Taking the derivative of Eq. (1) with respect to time produces Eq. (2), where the derivative with respect to time is indicated by dot notation.

$$\dot{E}_{mech} = \dot{m}g_0h + m\dot{g}_0h + mg_0\dot{h} + \frac{1}{2}\dot{m}V_{TAS}^2 + mV_{TAS}\dot{V}_{TAS} \quad (2)$$

To obtain the TEM from Eq. (2), it is assumed that the time derivatives of the mass and gravitational acceleration terms can be treated as effectively zero (i.e., $\dot{m} \approx \dot{g}_0 \approx 0$) and that the time derivative of the total energy expressed by Eq. (2) is equal to the rate of work (i.e., power) performed on the vehicle by thrust (T) and drag (D) forces aligned with the direction of travel (i.e., $\dot{E}_{mech} = TV_{TAS} - DV_{TAS}$). Thus, the TEM shown in Eq. (3) expresses the relationship between total power due to ‘‘thrust’’ and ‘‘drag’’ and associated changes in energy.

$$TV_{TAS} = DV_{TAS} + mg_0\dot{h} + mV_{TAS}\dot{V}_{TAS} \quad (3)$$

The individual terms of Eq. (3) are often reorganized and expressed differently depending on modeling needs, as discussed in detail in Ref. [10].

In the BADA H model for helicopter performance, the thrust and drag terms of Eq. (3) are generalized somewhat and shown in Eq. (4).

$$P_{eng} = P_{req} + mg_0\dot{h} + mV_{TAS}\dot{V}_{TAS} \quad (4)$$

Here, the thrust power term TV_{TAS} is replaced by P_{eng} representing the engine power, while the DV_{TAS} term is replaced by P_{req} , representing the power required by the flight condition excluding any power captured by the other terms. It is often useful to express the TEM in terms of horizontal and vertical components of velocity based on the relation

$V_{TAS} = \sqrt{V_{horiz}^2 + \dot{h}^2}$. It is easily shown that this leads to the form shown in Eq. (5).

$$P_{eng} = P_{req} + (mg_0)\dot{h} + (m\dot{h})\dot{h} + (mV_{horiz})\dot{V}_{horiz} \quad (5)$$

An advantage of this form is that the slope of the power requirement for vertical acceleration and horizontal acceleration is shown to be directly proportional to the velocity in the corresponding direction, while the power associated with maintaining a given climb velocity (\dot{h}) is proportional to the weight of the vehicle (mg_0). Recall that this model provides a substantially simplified expression of changes to total energy and does not explicitly account for the ways that the P_{req} term may also be influenced by velocity, acceleration, atmospheric effects, mass, turn-rate, or other factors not accounted for in the point-mass model. Nevertheless, these simple relations still provide insight into how the power-requirement will vary during climbs, descents, and accelerating flight, and is helpful for creating a performance model structure for UAM vehicles.

C. Power Requirement Modeling

Because the BADA 3 and 4 families are specifically designed to model the performance of fixed-wing aircraft, several simplifying assumptions are made that limit their applicability to other aircraft such as UAM vehicles. For example, in straight-and-level unaccelerated flight, the BADA 3 model assumes the power requirement is proportional to drag multiplied by true airspeed as shown in Eq. (3), and that the relationship between lift and drag is given by Eq. (6).

$$C_L = \frac{2mg_0}{\rho(V_{TAS})^2 S \cos(\phi)}, \quad C_D = C_{D0} + C_{D2}(C_L)^2 \quad (6)$$

In the lift coefficient (C_L) equation, mg_0 is the weight of the aircraft, ρ is the air density, S is the wing reference area, ϕ is the bank angle (typically computed based on a required turn rate), and V_{TAS} is the true airspeed. In the drag coefficient (C_D) equation, the values of C_{D0} and C_{D2} are parameters that are fit to available performance data and can vary with vehicle configuration such as during approach or landing. In addition to Eq. (6), models for jet, turboprop, and piston engines are provided that relate power or thrust requirement to fuel burn. See Ref. [10] for additional details. This simple model is often sufficient for fixed-wing aircraft operating at conditions within the nominal flight envelope. However, Eq. (6) would clearly be inappropriate for UAM vehicles operating in rotorcraft or hybrid flight modes due to an inability to accurately model performance in hover or slow flight.

The BADA 4 models utilize equations similar to those in Eq. (6) but with more parameters available to fit the performance data. For example, up to fifteen coefficients are included for the drag coefficient calculation, and the engine models are also more detailed than in BADA 3. While BADA 4 allows more accurate performance modeling than BADA 3 for airplanes, the mathematical structure underlying the model still assumes performance and operational trends which are not suited to UAM vehicle performance.

The BADA H model family shares many features with the BADA 3 and 4 models but replaces some of the fixed-wing assumptions with a model that is more suitable to rotorcraft flight performance and operations. For example, the power requirement in straight and level unaccelerated flight is proportional to C_{Preq} in Eq. (7).

$$C_T = \frac{mg_0}{\pi R^2 (\Omega R)^2}, \quad C_{Preq} = c_1 + c_2 \mu^2 + c_3 C_T \sqrt{\mu^4 + C_T^2 - \mu^2} + (c_4 + c_5 C_T^2) \mu^3 \quad (7)$$

In the thrust coefficient (C_T) equation, several terms are defined identically to Eq. (6), with ΩR representing the rotor tip speed (angular velocity Ω , rotor radius R) which is assumed constant. This assumption means that C_T is also assumed constant for a given mass and air density. The dimensionless velocity (μ) in C_{Preq} is given as $\mu = V_{TAS}/\Omega R$, which then varies only with the speed of the aircraft. The coefficients c_1 through c_5 in Eq. (7) are fit to the available performance data for the aircraft being modeled and provide sufficient degrees of freedom to capture the performance trends of traditional helicopters [12]. However, this model is not intended to capture the performance trends of UAM vehicles, particularly those that are designed to transition into fixed-wing or hybrid flight modes at higher airspeeds.

An attempt at modeling a tiltwing-type UAM vehicle using a model based on BADA H is described in Ref. [13]. Here, the assumption in Eq. (7) of constant rotor speed is dropped and replaced by a fifth order polynomial defined as a function of (V) as shown in Eq. (8).

$$\Omega(V) = \sum_{i=0}^5 c_i V^i \quad (8)$$

It is noted in Ref. [13] that the motivation for this polynomial model is not to capture realistic rotor-speed variations, but rather as an empirical model that adds sufficient degrees of freedom to Eq. (7) to model the unique performance variation seen during the transition from hover to forward flight of the particular UAM vehicle considered.

D. Operations and Procedures

Additional modeling assumptions and simplifications are made in BADA models in order to specify the operations and procedures that will be followed by the aircraft. For BADA 3 and 4, these assumptions are consistent with typical fixed-wing operations and include climb and cruise speed schedules, stall speeds, descent speeds, and others. Similar assumptions are included in BADA H, with modifications made to accommodate standard helicopter operations. Appropriate assumptions for UAM operations are still largely unknown, as typical flight segments are not well established, ATM procedures are still being determined, and vehicles are being designed to target different mission profiles and operations. Accommodating this uncertainty in UAM operations and procedures may necessitate a more

flexible approach to defining operations and procedures within the performance model than has previously been required.

E. Performance Table File

The BADA 3 PTF and PTD files contain performance data that is generated based on the parametric models described by the OPF and APF files. Individual flight segments such as “climb” and “cruise” are included, and key flight performance details such as airspeed, fuel burn, and climb or decent rate are provided as a function of altitude and payload in an easy-to-read table format. The PTF and PTD thus provide a convenient representation of the aircraft’s nominal performance, and for some applications can provide sufficient information as a stand-alone source of basic performance data. Additionally, the format allows for straightforward comparison of aircraft performance characteristics and can support basic calculations related to time enroute and fuel burn.

F. Applicability of Common Performance Modeling Methods to UAM Vehicles

While some elements of the BADA model formats have direct applicability to UAM vehicles and operations, many are not compatible. For example, the basic assumption of a point-mass TEM as the foundation of power consumption calculations can be adapted to UAM performance modeling, particularly if a form such as Eq. (4) or (5) is used. Additionally, an overall file structure similar to BADA models can likely be used for modeling UAM vehicles if this is deemed desirable, particularly as UAM operations and ATM procedures for these aircraft become better defined. However, appropriate power requirement equations comparable to Eqs. (6)-(8) for UAM vehicles are not apparent, and existing examples (e.g., Ref. [13]) are limited in applicability. This leaves performance modelers for UAM vehicles with no widely accepted modeling methodology or structure to apply. For the present work, assuming a specific regression model describing UAM flight performance and operations was avoided, as this seemed premature and potentially limiting. As discussed in Section IV, a performance model based on an adapted Performance Table format in conjunction with locally defined parametric models was found to offer adequate flexibility for capturing UAM vehicle performance over the flight envelope of interest.

III. Performance Data

Existing performance modeling formats, such as BADA, are generally used to create models for vehicles already flying in the real world. The models are developed using a combination of publicly available data and, if available, manufacturer data. For existing commercial fixed-wing and rotorcraft vehicles, this approach has worked well and produced valuable performance models. However, UAM vehicle designs are new and rapidly evolving, and most manufacturer’s performance data are currently unavailable. At the same time, regulators are still developing flight worthiness requirements and ATM procedures, creating some remaining uncertainty as to how these vehicles will need to be designed and operated. These factors necessitated the development of a novel approach to obtaining representative UAM performance data.

NASA developed a series of UAM conceptual vehicle designs to study tradeoffs and quantify performance targets suitable for guiding the implementation UAM systems [5]. Figure 1 shows the vehicles that provide the basis for the performance models outlined in this paper. Each of these vehicles were created to demonstrate combinations of features being analyzed for UAM aircraft. These UAM concepts are publicly available from NASA [15]. The conceptual vehicles’ NDARC models allow performance data generation for a vast array of flight conditions. Examining the data enables the creation of representative vehicle performance models usable for ATM systems analysis.

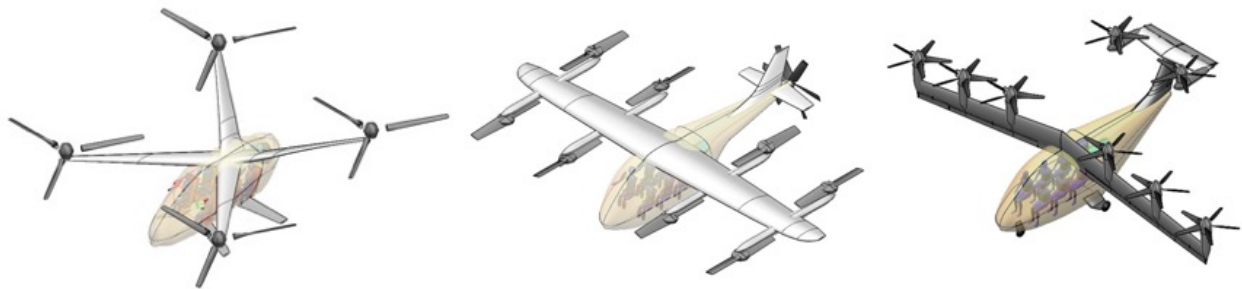


Fig. 1 NASA conceptual UAM vehicles selected for performance modeling: the six-passenger Quadrotor, Lift+Cruise, and Tiltwing aircraft designs.

A. Sizing Mission

The NASA UAM vehicle concepts are designed and sized to meet the mission requirements proposed in Ref. [5]. The sizing mission calls for a payload of six passengers carried on a 75-mile round trip without the need to refuel or recharge the vehicle's batteries. The mission assumes a passenger weight with baggage of 200 lb each, for a total payload weight of 1,200 lb. The sizing mission uses a 10-knot headwind during each cruise segment, and the vehicle is required to possess an energy reserve equivalent to 20 minutes of additional cruise flight. The vehicle must be able to operate from a 6,000 ft International Standard Atmosphere (ISA) takeoff altitude and cruise at 4,000 ft above ground level (10,000 ft ISA). The vehicle is also sized to hover out of ground effect (OGE) and vertically ascend and descend at 100 ft/min during vertical take-off and landing operations. Motor sizing for the aircraft is primarily driven by the hover and vertical take-off requirement at 6,000 ft, while the vehicles' energy capacities (i.e., battery and fuel tank size) are largely driven by the round-trip cruise distance and reserve requirements previously discussed.

B. Vehicle Descriptions

Figure 1 shows the NASA UAM concepts selected for generating vehicle performance models. Table 2 provides a brief description of these vehicles. More detailed descriptions of the NASA concepts can be found in Refs. [2–4]. NASA designed several quadrotor variants to compare different powertrain configurations. The Quadrotor performance model in this paper was based on an electric six-passenger variant with collective-controlled rotors and cross-shafting between rotors to transmit and distribute power from all four motors to each rotor.

Table 1 Performance Model Vehicle Properties.

Vehicle	Quadrotor	Lift + Cruise	Tiltwing
Powertrain	Electric	Electric	Hybrid Turboelectric
Number of Lifting Rotors	4	8	8
Max. Rated Power (MRP) per Lifter, hp	168	134	227
Lifter Radius, ft	13.1	5.0	3.7
Number of Cruise Rotors	-	1	8
MRP per Cruise Rotor, hp	-	535	-
Cruise Rotor Radius, ft	-	4.5	-
Wingspan, ft	-	51	44
Wing Area, ft ²	-	217	128
L/D _e	5.8	8.5	8.72
Design Gross Weight, lb.	6,470	7,477	6,716
Operating Empty Weight, lb.	5,270	6,277	5,516
Useful Energy Capacity, MJ	1,325	1,220	4,738
Battery, MJ	1,325	1,220	212
Fuel Tank, lb.	-	-	250

The NASA electric Lift+Cruise follows a conventional General Aviation (GA) aircraft layout with eight fixed-pitch rpm-controlled rotors powered by individual electric motors and mounted to the wing to enable VTOL performance. A rear mounted variable-pitch propeller powered by an electric motor provides forward propulsion. Control of the wing-mounted lifting rotors are mixed to enable multirotor like operations at low speeds during VTOL. The wing motors are intended to be stopped and stowed in a low drag position while the vehicle operates in cruise. Standard fixed-wing aircraft control surfaces (ailerons, elevator, and rudder) are provided for use during cruise flight.

The NASA Tiltwing is a hybrid turboelectric vehicle with a conventional GA aircraft layout with six rotors fixed to the main wing and two rotors mounted to the horizontal tail. This configuration tilts the entire wing to a vertical position to achieve VTOL capability. The tail rotors tilt as well, but the horizontal tail and motor nacelle stay fixed. This vehicle uses a distributed electric propulsion system powered using a turboelectric generator. An additional battery is included to provide a power reserve in the case of engine failure. The rotors of the Tiltwing are controlled by their individual collectives. The rotors also change speed depending on the vehicle's flight mode. The rotors operate at a tip speed of 550 ft/s at hover and during transition to forward flight and are slowed to 300 ft/s tip speed during cruise flight to reduce noise. The collectives of the individual rotors are mixed to enable multirotor-like flight control when operating in VTOL. The vehicle also has conventional fixed-wing control surfaces including ailerons, elevator, flaps, and rudder.

C. Generating and Analyzing Performance Data

A performance database for each vehicle was generated covering a broad range of payloads, altitudes, airspeeds, and flight modes. The data was obtained using NDARC to conduct trim sweeps over specified conditions, where for example payload, altitude, acceleration, and rate-of-climb were held constant while sweeping the airspeed through values of interest. At each condition, NDARC would attempt to trim the vehicle as defined by the *trim quantity* (often a selection of relevant forces and moments to be zeroed), using the available degrees of freedom and flight controls specified as the *trim variables*, and using an initial guess supplied to the numerical solver. The output of the performance sweep is a text file containing detailed aircraft performance information for each trim condition where a solution was obtained.

A MATLAB® script and related functions were written to manage the large number of NDARC runs needed to build a performance database for each aircraft. The script sweeps over the complete range of conditions required to generate the performance data and organizes the output files. In many cases, runs needed to be performed multiple times with different trim settings and solver guesses to obtain performance data over the flight conditions of interest. For vehicles with multiple distinct operating and control modes (e.g., “hover/multirotor”, “transition”, “fixed-wing cruise”) such as the Lift+Cruise and Tiltwing aircraft, data for each flight mode was obtained through separate NDARC runs and then analyzed to determine appropriate operating envelopes and applicability for each flight mode. The output files from successful trim runs were parsed and post-processed into a large MATLAB “table” structure to facilitate analysis of the performance data. This database was then analyzed to establish a nominal flight envelope and select appropriate conditions for defining specific flight segments, such as optimal cruise airspeeds or climb configurations.

D. Trim Definitions and Optimization

It is important to ensure that the trim definitions and degrees-of-freedom in the control system are appropriately applied for each aircraft and flight condition when generating the performance database. NDARC does not have a built-in capability to solve trim-optimization problems, which might be more frequently encountered in UAM vehicles where redundant actuation or degrees-of-freedom are present, or where trim solutions are otherwise not unique. NDARC requires that any excess degrees-of-freedom must be removed before trimming, such that the number of free variables used to trim the aircraft is equal to the number of constraints. NDARC also lacks the ability to explicitly search for a trim that minimizes an objective function, such as minimizing power requirement or control effort. One approach to overcoming these limitations is to reduce the excess degrees-of-freedom by implementing a control mixing strategy such that the available effectors are mixed to the aircraft controls, which NDARC supports through specification of a control mixing matrix. This matrix must be specified by the user and can be defined to vary with flight condition. In addition, excess trim variables can be manually fixed to a desired value or programmed to vary with flight condition in a prescribed manner prior to executing the performance calculation in NDARC.

Basic performance modeling will often require data describing forward flight of the aircraft at a specified airspeed, altitude, payload, and climb rate with zero acceleration. If no sideslip and vehicle symmetry about the body x-z plane are assumed, the trim quantities can be defined by setting the total force in the vertical and horizontal directions and total pitching moment to zero. This creates three total constraints (trim quantities) such that NDARC will accept three unknown trim states or controls (trim variables) as part of the trim computation task. Additional degrees of freedom in the problem (such as redundant effectors) are not compatible with the NDARC trim routine and must be eliminated either by fixing the value of the variable, or by providing a control mixing scheme that reduces the degrees of freedom down to the number of trim quantities. Table 2 provides a comparison of the trim variables and control effectors available for each of the three vehicles in this scenario.

Table 2 Comparison of available trim variables and control effectors during transition.

Vehicle	Trim Variables: flight states and controls used to trim during transition
<i>Quadrotor</i>	pitch, distributed collective, fore-aft rotor thrust difference
<i>Lift+Cruise</i>	pitch, distributed rotor rpm, fore-aft rotor thrust difference, pusher-prop thrust, elevator
<i>Tiltwing</i>	pitch, distributed collective, fore-aft rotor thrust difference, tilt, elevator, flaps

Table 2 shows that after basic control mixing is applied, the Quadrotor has only three relevant trim variables in forward flight, so there is no redundancy to eliminate if there are three trim quantities. However, both the Lift+Cruise and Tiltwing aircraft have additional trim variables that must be eliminated to be compatible with the NDARC trim routine for the case of three trim quantities. Power requirement is determined implicitly based on the other variables.

For the Lift+Cruise vehicle, the elevator control surface creates a redundant control for pitch moment during transition where there is also a controllable pitch moment from thrust differential between the fore and aft wing-

mounted rotors. Additionally, the pitch attitude of the vehicle influences both main-wing and horizontal stabilizer angle of attack while also tilting the net thrust vector from the wing-rotors. Simultaneously, thrust is also generated by the pusher-prop, creating coupled redundancy in the vertical and horizontal force-control trim variables. To eliminate these redundancies, performance sweeps were computed throughout the range of transition airspeeds (roughly 0 to 85 knots) over a discrete range of pitch angle increments while fixing the elevator at zero. The resulting data was post-processed to determine a nearly minimum-power pitch profile to be used during transition. This approach was motivated by the large effect pitch angle had on power requirement, and the relatively small influence that elevator appeared to have. While the simplicity of this approach is desirable, it does not extend well to vehicles with more complex forms of trim-variable redundancy.

A different approach was required to trim the Tiltwing vehicle throughout the range or transition airspeeds. As listed in Table 2 and illustrated in Fig. 2, the trim variables for the Tiltwing include the angle between the inertial x-axis (x_i) and body x-axis (x_b) as pitch (θ), distributed collective angle (which influences total thrust $T_1 + T_2$), fore-aft rotor thrust difference (which influences $T_1 - T_2$), main wing and tail-rotor tilt (τ), elevator (δ_e), and flaps (δ_f). The center of mass (CM) is also shown in red.

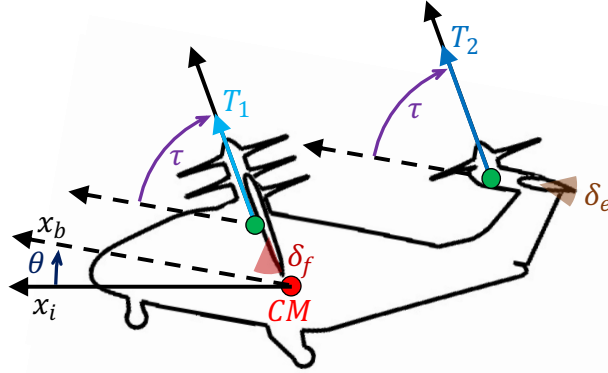


Fig. 2 Diagram of available trim variables used for tiltwing during transition. Drawing not to scale.

To optimize the trim configuration throughout transition, the MATLAB Optimization Toolbox™ function “fmincon” was used to iteratively execute NDARC trim tasks, with the goal of solving a nonlinear constrained optimization problem. At each flight condition of interest, NDARC was used to trim using the variables pitch, distributed collective, and fore-aft rotor thrust difference, while MATLAB sought to optimize over the range of available values of tilt, elevator, and flaps. This approach relied on several purpose-created scripts to enable MATLAB to interface with NDARC. During each optimization attempt, MATLAB calls NDARC multiple times to compute local gradients for the objective function and returns a solution when the local gradient indicates a minimum has been found. While there is no guarantee of global optimality using this approach, the results were analyzed and appeared feasible, locally optimal, and adequately efficient. The objective function for the optimization is shown in Eq. (9), with the cost (J) defined to reflect a primary goal of minimizing total power requirement at the trim condition (P_{trim}) while also ensuring reasonable pitch attitude and elevator and flap angles. Note that while τ does not appear explicitly in the cost expression, it implicitly influences the value of P_{trim} and the other trim variables.

$$J(\tau, \delta_f, \delta_e) = P_{trim} + k_\theta \theta^2 + k_e \delta_e^2 + k_f \delta_f^2 \quad (9)$$

For the purposes of computing optimal trim configurations, τ was constrained to values between 0° and 90° , elevator to $\pm 20^\circ$, and flap angle to between 0° and 40° . The objective function cost was set to penalize non-zero pitch angle (θ) at hover and low airspeeds, with a pitch-cost coefficient (k_θ) computed as a linearly decreasing function of calibrated airspeed that reached zero at 90 knots. The other cost coefficients were fixed values, with the coefficient k_e penalizing elevator deflection and k_f penalizing flap angle. These coefficients were chosen to be very small relative to the P_{trim} and pitch cost but were included to create a bias toward minimal control surface deflection at conditions where the control surfaces have little influence on the power requirement of the trim solution. No additional cost was explicitly assigned to tilt, collective thrust, or fore-aft thrust difference. These inputs influence P_{trim} but are not otherwise penalized. It is notable that the NASA Tiltwing was not sized to meet any specific design criteria throughout transition, and that changes to the design influencing vehicle geometry or control effectiveness could have a substantial impact on the optimal transition profile for the aircraft.

This method of optimization was computationally expensive, so only selected conditions were studied and a near-optimal schedule for transition was created. Optimal transitions in terms of τ , δ_f , and δ_e were computed for unaccelerated level flight in one knot increments of calibrated airspeed at several different altitudes. The routine performed a marching sweep in order of increasing airspeed, using the previous trim as an initial guess to the solver. Near hover, a flap setting of 20° coupled with a tilt angle of about 75° was found to require minimum power due to the aerodynamic effects of the propeller downwash on the wings. At low speeds δ_e had a negligible effect, while at higher speeds approaching the completion of transition the optimal solution required about 20° elevator deflection. A transition schedule was synthesized from analyzing these optimal runs, such that θ , and δ_f were taken as functions of V_{CAS} while δ_e was held constant at 20° , as shown in Fig. 3. This transition schedule was then used to compute the performance database for the Tiltwing vehicle. For flight conditions where both transition-mode and airplane-mode ($\tau = 0^\circ$) trims were available, the airplane mode trims were used for developing the performance model as these required less power and better reflected realistic aircraft operation. This approach produced near-optimal power requirement throughout the transition range of airspeeds and was effective for the purposes of this modeling effort. A limitation of this approach was the assumption of level-altitude, unaccelerated flight. Optimality of this schedule under substantial acceleration or rates of climb or descent was not studied in detail. More in-depth analysis of transition flight would be necessary for applications involving vehicle design and high-fidelity modeling.

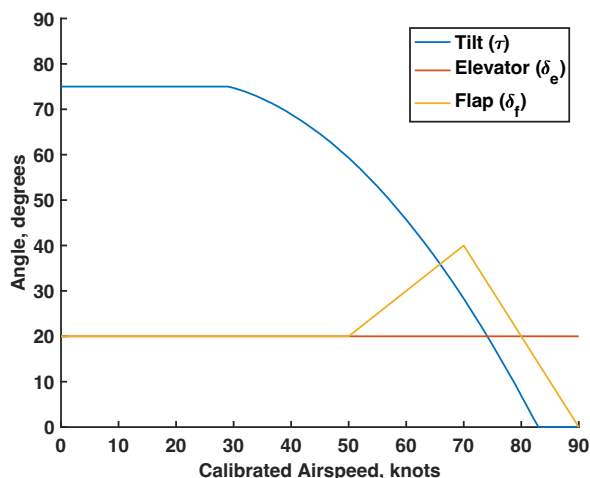


Fig. 3 Specified schedule of Tiltwing tilt (τ), flap (δ_f), and elevator (δ_e) used for transition.

E. Climbs and Descents, Acceleration, and Turns

The preceding discussion considered computing trims and performance under zero acceleration and level-flight conditions. The power requirement under horizontal and vertical acceleration, turns, and climbing and descending flight is also of interest. The TEM shown in Eqs. (3)-(5) includes terms directly related to climb or descent rate and acceleration power. However, these terms alone are insufficient to capture the full power impact of climb rate and acceleration, and for UAM vehicles the power requirement during these maneuvers must be accounted for by the other power requirement terms, such as P_{req} in Eq. (4).

Climbing and descending performance was studied in NDARC using sweeps over a wide range of airspeeds and climb or descent rates. An example for the Quadrotor is shown in Fig. 4 (a). Maximum rated power (MRP, limited to 10 min) and maximum continuous power (MCP, no time limit) boundaries are shown, as is the approximate zero-power boundary, which would likely manifest as onset of autorotation in this aircraft. For this vehicle design, the MRP motor rating was assumed to be 150% of the MCP [3]. Note the nonlinear performance variation over the flight envelope, particularly at low airspeeds. At airspeeds near hover, high power is required to maintain altitude, with reduced power required at intermediate speeds below cruise. From the figure it is apparent that for this payload and altitude the maximum climb rate when limited to MCP is achieved near a horizontal speed of 50 knots. At low-speeds, a nonlinear relationship between climb rate and power is apparent, but at higher speeds the relationship between climb rate and power appears nearly linear, as indicated by vertically equidistant spacing between the power-required contour lines. Analysis of the Quadrotor flight envelope is straightforward in comparison to the more complex UAM designs due to the lack of a fixed-wing flight mode, and the presence of cross-shafting between motors which simplifies the analysis of power requirement limitations.

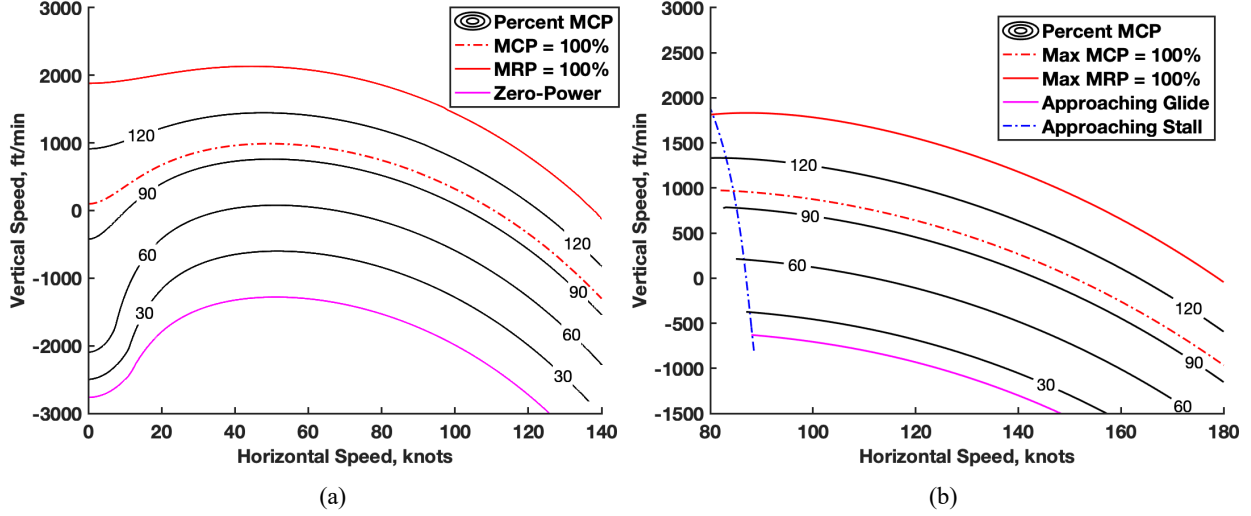


Fig. 4 Quadrotor (a) and tiltrotor in airplane mode (b) power requirement for carrying six passengers at sea level ISA conditions. Note difference in scale of axes between (a) and (b).

Figure 4 (b) shows maximum power requirements in climb and descent for the Tiltwing vehicle operating in an airplane flight configuration with the tilt of the main wing and tail tiltrotors fully horizontal. Here, the maximum power requirement is defined as being the maximum across all the motors present on the aircraft, since there is no cross shafting. As expected, the trends observed correspond to typical fixed-wing aircraft performance, in contrast to the helicopter-like performance of the Quadrotor shown in Fig. 4 (a). Note that at higher speeds in Fig. 4 (a), the general trends in power requirement are similar to Fig. 4 (b). Transition conditions associated with lower airspeeds are omitted from Fig. 4 (b) because the limiting factors for a given airspeed and climb or descent rate are a strong function of trim selection and control allocation, leading to difficulty in generalizing the results to produce meaningful envelope boundaries or trends. For example, the choice of trim in this flight region has a substantial impact on which trim variables (such as motor power) first saturate near the boundaries of the feasible flight envelope. Because NDARC does not include tools suitable for studying this problem, determination of feasible flight envelopes during transition remains an issue for further exploration in future work.

To analyze vehicle performance during acceleration, selected flight conditions corresponding to individual segments of flight were analyzed in NDARC. Acceleration sweeps were performed over a range of selected acceleration magnitudes and angles relative to the vehicle’s body-axes. Trim conditions with acceleration in the body x - z plane (horizontal and vertical, with no sideward acceleration) ranging from 0.05 to 0.2 g ’s were computed over a finely spaced range of angles relative to horizontal, and the resulting data was analyzed to observe trends in the power requirement as well as the feasibility of the trim condition. It was noted that under most flight conditions, and for small acceleration values of up to about 0.2 g ’s, the power requirement was nearly linear in \dot{V}_{horiz} and \dot{h} for all three aircraft studied, agreeing with the basic linear form of the corresponding terms in Eq. (5). However, the coefficients given in the TEM for these terms (mV_{horiz} and $m\dot{h}$ respectively) do not account for the observed slope of the power requirement, motivating the more general coefficient formulation introduced in Section IV.

F. Performance Discussion

The data obtained from NDARC was sufficient to support basic performance modeling throughout the nominal flight envelope and allowed limited analysis of off-nominal conditions. Fig. 5 (a) shows a comparison of the power requirement in straight and level unaccelerated flight as a function of airspeed at sea-level ISA conditions with six passengers. The vertical axis shows the power draw or fuel consumption rate for flight at a given airspeed, normalized by the available storage in the battery or fuel tank. This normalization facilitates a comparison of the relative power-requirement trends observed for the fully electric and turboelectric aircraft considered here. Conditions resulting in a lower energy consumption rate correspond to increased endurance capability, which can be seen in Fig. 5 (b). The Lift+Cruise design is observed to have the poorest endurance in hover, while the Quadrotor performs best in this regard. This is expected, as more traditional helicopter designs tend to be well-suited to missions involving prolonged hovering flight. Maximum endurance for the Lift+Cruise and Tiltwing designs is obtained at the transition point to fixed-wing flight, near 90 knots for these conditions. For the Quadrotor, maximum endurance occurs at a lower speed,

with an overall trend closely comparable to that of traditional rotorcraft. The power requirement trends for the Quadrotor can be reasonably well modeled using the BADA H power equations described in Ref. [12] and given here as Eq. (7). However, it can be easily inferred from Fig. 5 (a) that Eq. (7) is not well-suited to modeling either the Lift+Cruise or the Tiltwing vehicle due to the more complex and nonlinear variation in power requirement during transition.

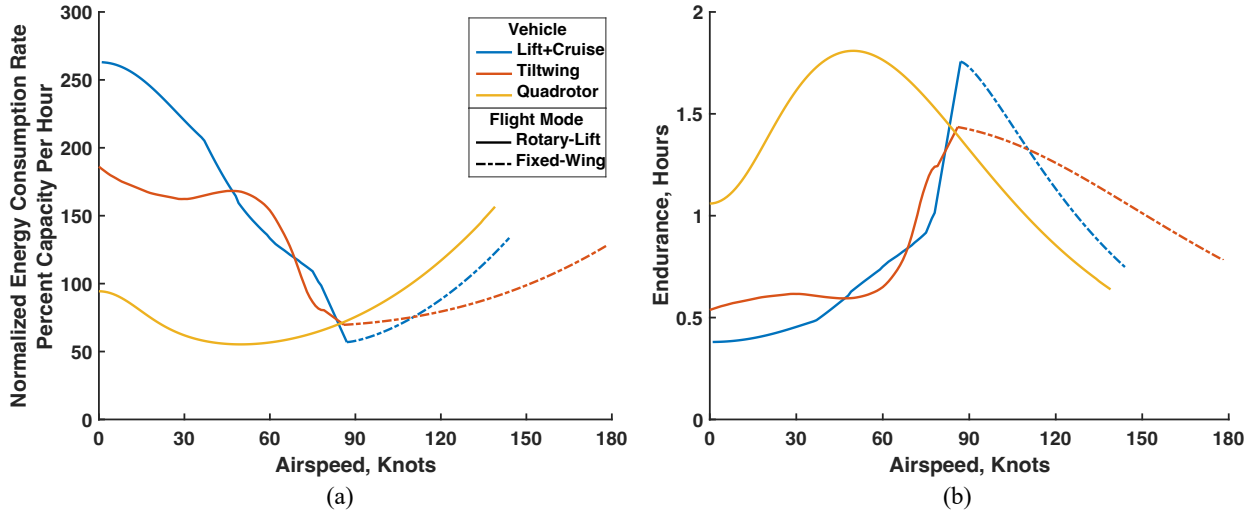


Fig. 5 Comparison of power/fuel consumption (a) and endurance (b) for level unaccelerated flight with six passengers at sea level ISA conditions.

Also of interest is range, shown in Fig. 6, based on assuming a fully charged battery or full fuel tank, six passengers, and sea-level ISA conditions. The range shown is based simply on power/fuel consumption at the specified condition and does not represent the actual range capability that would be realized for a complete mission. It is notable that the Tiltwing experiences its best range efficiency at significantly higher speeds than either the Lift+Cruise or Quadrotor. The Lift+Cruise design has higher maximum range than the Quadrotor, but this occurs at speeds only slightly higher, indicating that flight time would be similar. It should be noted that these vehicle characteristics are the result of not only the vehicle design type (i.e., Quadrotor, Lift+Cruise, Tiltwing), but also the design details and the specific sizing mission that was implemented. Changes to the sizing mission could have a profound effect on the relative performance of the vehicles, so broad generalizations about relative strengths and weaknesses of vehicle designs based solely on this data are not appropriate. In contrast, Ref. [16] demonstrates an approach to comparing vehicle design suitability as a function of intended mission parameters.

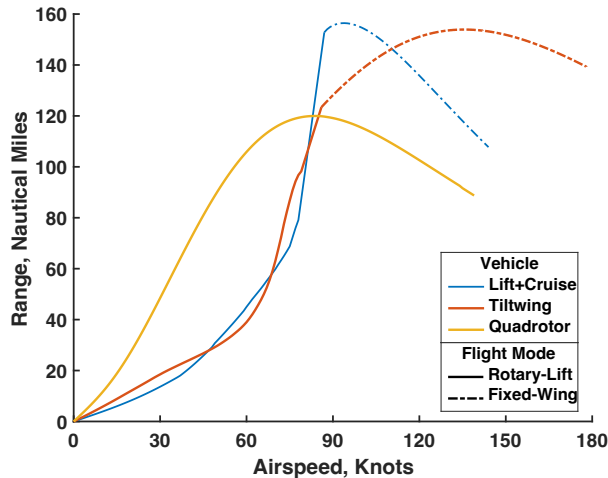


Fig. 6 Comparison of range for level unaccelerated flight with six passengers at sea level ISA conditions.

The complex variation in power requirement with airspeed depicted in Fig. 5 illustrates one of the primary challenges of performance modeling for UAM vehicles. Each vehicle’s performance is heavily dependent on the aircraft’s unique design characteristics and operating mode, as well as choices about how nominal trajectories and operations for the aircraft are defined. Together, these characteristics create challenges for performance modeling purposes.

IV. Performance Model

The disparate performance trends among UAM concepts led to the selection of a performance modeling approach comparable in format to the PTF tables provided with BADA models [9], adapted and expanded to suit UAM vehicle performance and operations. This approach was selected to support the goal of maximizing the relevance and accuracy of the model data provided to users, while avoiding issues associated with creating suitable parametric models for describing UAM vehicle performance and operations over their full envelopes. The mission segments included in the performance tables were selected to capture vehicle performance during anticipated UAM flights. The tables contain data that directly represents nominal operations based on analysis of the performance database generated using NDARC. Nominal airspeeds for segments were specified in terms of a calibrated airspeed (CAS), similar to the approach taken in BADA models [10]. An overview of the segments included is provided in Table 3.

Table 3 Performance Table Segment Descriptions

Segment Name(s)	Description
<i>Hover</i>	Out of ground effect (OGE) hover fuel/power requirement
<i>Vertical Climb/Descent</i>	Fuel/power requirement for ± 100 ft/min vertical climb/descent
<i>Low/Nominal Descent</i>	Fuel/power requirement for descent at selected low CAS or nominal cruise CAS
<i>Climb</i>	Maximum rate of climb at optimal CAS and maximum continuous power
<i>Transition</i>	Fuel/power requirement for level flight at a selected intermediate CAS
<i>Endurance Cruise</i>	Fuel/power requirement at optimal CAS selected for maximum endurance
<i>Nominal Cruise</i>	Fuel/power requirement at 99% “high-side” best range CAS for nominal cruise.
<i>Low/High Cruise</i>	Provides the fuel/power requirement at ± 10 knots nominal cruise CAS.
<i>MCP Cruise</i>	Maximum TAS possible for level flight at maximum continuous power (MCP).
<i>MRP Cruise</i>	Maximum TAS possible for level flight at maximum rated power (MRP)

The performance table provides a selection of data appropriate for each segment. Three payload classes are specified: low weight (lo) corresponds to one passenger (200 lb pilot only), nominal weight (nom) to four passengers (800 lb), and high weight (hi) to six passengers (1,200 lb). The three weight classifications are similar to those used in the BADA 3 PTF [10] and were defined identically for each vehicle, though in general the loadings would be adapted to the vehicle under consideration. For the fully electric Quadrotor and Lift+Cruise vehicle there is no weight change during flight due to fuel burn. For the Tiltwing aircraft, the change in weight due to fuel burn is easily accounted for via interpolation between the included payload weights. Altitude dependency of performance data is shown by rows in the data set corresponding to 1,000 ft increments of ISA condition. Each column is labeled and varies with flight segment. For example, in nominal cruise the performance data provided is TAS and fuel/power consumption rate as a function of altitude and payload. For the hover and vertical climb or descent segments, similar data is provided but with airspeed omitted as it is assumed zero. For the climb segment, TAS, rate of climb, and fuel/power consumption is provided as a function of weight and altitude. For the descent segment, an airspeed, descent rate, and fuel/power consumption rate are provided in terms of weight and altitude. For the MCP and MRP cruise segments, the columns contain maximum TAS and associated fuel burn as a function of altitude and weight. In this way, the performance tables provide a simple and concise description of each aircraft’s performance.

G. Climb Performance Modeling

Nominal airspeed selection for flight segments was accomplished based on an analysis of the available performance data. For example, the optimal calibrated airspeed for climb was selected based on targeting the maximum possible climb rate at MCP. To illustrate, Fig. 7 shows the maximum rate of climb achievable at MCP as a function of airspeed for the NASA Quadrotor at a variety of weights and ISA altitudes.

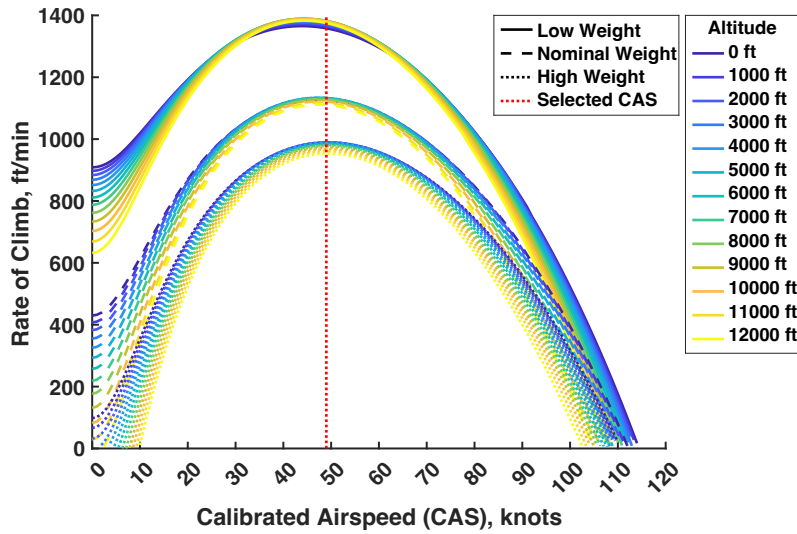


Fig. 7 Quadrotor rate of climb at MCP for a range of weights, altitudes, and calibrated airspeeds.

Note that altitude has limited impact on the achievable climb rate for this aircraft at calibrated airspeeds near 50 knots. Based on this performance, an airspeed of 49 knots (shown by the vertical dotted red line) was selected for the climb segment in the Quadrotor performance table. This airspeed provides optimal climb rate at MCP for six passengers while operating at 6,000 ft ISA and produces only slightly suboptimal climb rates at other weights and altitudes. The climb segment performance table for the Quadrotor is shown in Fig. 8, where “ROCD” stands for rate of climb or descent, TAS for true airspeed, and FL for flight-level. A similar analysis was performed for the Lift+Cruise and Tiltwing vehicles to determine the best climb airspeed and associated performance, where it was assumed that the climb would be performed in the fixed-wing operating mode.

FL	CLIMB				
	TAS [kts]	ROCD [ft/min]			fuel [MJ/hr]
		lo	nom	hi	
0	49.0	1358.2	1125.7	988.0	1376.8
10	49.7	1363.7	1128.5	989.2	1376.8
20	50.5	1368.5	1130.7	989.8	1376.8
30	51.2	1372.7	1132.2	989.6	1376.8
40	52.0	1376.1	1132.9	988.7	1376.8
50	52.8	1378.7	1132.9	987.0	1376.8
60	53.6	1380.6	1132.1	984.6	1376.8
70	54.4	1381.7	1130.5	981.4	1376.8
80	55.3	1382.0	1128.2	977.5	1376.8
90	56.1	1381.6	1125.1	972.8	1376.8
100	57.0	1380.4	1121.2	967.2	1376.8
110	57.9	1378.3	1116.4	960.7	1376.8
120	58.8	1375.4	1110.7	953.4	1376.8

Fig. 8 Climb segment from the performance table for the Quadrotor.

H. Cruise Performance Modeling

The nominal cruise airspeed was selected to correspond closely to the “99% high-side” optimal range airspeed for each aircraft, consistent with the cruise description provided in Ref. [6]. This choice of cruise airspeed trades a slightly suboptimal range for increased speed, decreasing required flight time while having minimal impact on range. Figure 9 provides a plot showing the Lift+Cruise vehicle’s range as a function of airspeed while operating with six passengers in airplane mode with the lift-rotors inactive, with range normalized by the percentage of maximum range at sea level ISA conditions. The selected nominal cruise speed of 99 knots CAS is shown in red. As altitude increases, both the range and true airspeed are increased due to decreased air density. It is notable that in fully electric aircraft there is often no change in available power with altitude, which is not the case for many piston or turbine powered air-breathing

engines, such as the turbo-electric Tiltwing. Additionally, several other cruise segments are defined to expand the flexibility of the model. These include the transition, maximum endurance, low speed, high speed, and MCP and MRP cruise segments as described in Table 3.

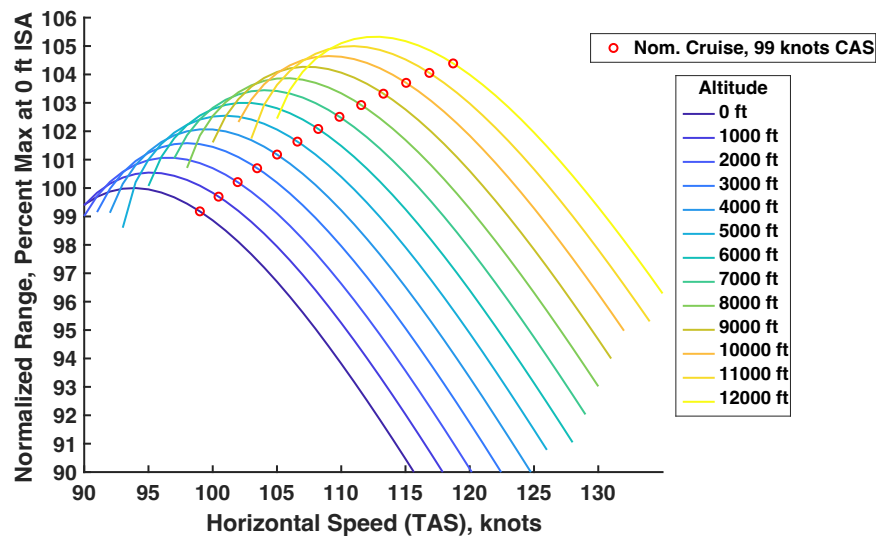


Fig. 9 Normalized range for nominal cruise for Lift+Cruise with six passengers. Selected speed of 99 knots CAS indicated in red.

FL	NOMINAL CRUISE			
	TAS [kts]	fuel [MJ/hr]		
		lo	nom	hi
0	99.0	719.2	755.9	783.1
10	100.5	725.5	762.8	790.5
20	101.9	732.0	769.9	798.1
30	103.5	738.7	777.4	806.0
40	105.0	745.8	785.1	814.2
50	106.6	753.1	793.1	822.8
60	108.2	760.7	801.4	831.6
70	109.9	768.6	810.0	840.8
80	111.6	776.8	819.0	850.3
90	113.3	785.2	828.2	860.1
100	115.1	794.0	837.8	870.3
110	116.9	803.1	847.7	881.0
120	118.7	812.5	858.0	892.1

Fig. 10 Cruise segment from the performance table for the Lift+Cruise.

The MCP and MRP cruise segments differ in format from the other cruise segments. For these, the table contains the maximum achieved true airspeed and associated fuel consumption rate as a function of altitude and payload while operating at either MCP or MRP power settings. This table is included to provide a precise capture of the upper limit of airspeeds available for the aircraft. An example of the MCP cruise performance table entry for the Tiltwing is shown in Fig. 11.

FL	MCP CRUISE			
	TAS [kts]			fuel [lb/hr]
	lo	nom	hi	
0	154.38	152.4	150.9	271.8
10	155.77	153.7	152.2	267.5
20	157.17	155.1	153.5	263.4
30	158.6	156.4	154.7	259.4
40	160.05	157.8	156.1	255.5
50	161.51	159.2	157.4	251.7
60	162.99	160.6	158.7	248.1
70	164.5	162.0	160.0	244.6
80	166.02	163.4	161.3	241.3
90	167.55	164.8	162.7	238.0
100	169.08	166.3	164.0	234.8
110	170.66	167.7	165.4	231.8
120	172.24	169.2	166.8	228.8

Fig. 11 Maximum continuous power cruise segment from the performance table for the Tiltwing aircraft.

I. Computing Performance at Arbitrary Flight Conditions

In some applications, it will be necessary to compute vehicle performance at conditions not listed in the performance tables. In the simplest cases, this can be accomplished via interpolation between nearby flight conditions. An example would be using successive linear interpolation to find the fuel burn rate for an airspeed between “nominal cruise” and “high cruise”, at an altitude of 2,500 ft ISA, and with a payload corresponding to two passengers. For many steady-state flight conditions of interest, this approach is straightforward and produces accurate results. However, for circumstances involving substantial acceleration, turning flight, or an arbitrary climb or descent rate, interpolation from nearby conditions might be insufficient.

To address this need, parametric models are provided that enable calculation of performance beyond those flight conditions that are explicitly listed. These models provide the power requirement for an arbitrary climb or descent rate and during accelerated flight and turns. The total power (P_{total}) is computed as a sum of four terms: unaccelerated flight with no bank angle ($P_{ss,level}$) derived from the performance table, power required due to a banked turn (P_{bank}), power required for an arbitrary climb or descent rate (P_{ROCD}), and power required due to acceleration (P_{accel}), as shown in Eq. (10).

$$P_{total} = P_{ss,level} + P_{bank} + P_{ROCD} + P_{accel} \quad (10)$$

Comparing this form with the TEM equation given as Eq. (3) and the subsequent Eq. (6), note that the $P_{ss,level}$ and P_{bank} terms together will correspond closely to the DV_{TAS} term, P_{ROCD} to the $mg\dot{h}$ term, and P_{accel} to the $mV_{TAS}\dot{V}_{TAS}$ term. The terms in Eq. (10) however are intended to be adapted to the vehicle under consideration and must serve a more generalized purpose than the point-mass model terms of Eq. (3) or (4). Each of the power terms on the right-hand side of Eq. (10) are computed using empirically determined parameter values that in general can be defined to vary with flight segment, altitude or atmospheric conditions, velocity, and weight.

For example, the P_{bank} term was defined as given in Eq. (11).

$$\phi = \text{atan}\left(\frac{V_{TAS}\dot{\psi}}{g}\right), \quad P_{bank} = m\left(\frac{1}{\cos(\phi)} - 1\right)k_{bank} \quad (11)$$

Given a desired turn rate ($\dot{\psi}$), airspeed (V_{TAS}), and gravitational acceleration (g), the required bank angle (ϕ) can be computed, which is then used to compute P_{bank} using the vehicle mass (m) and an empirical coefficient (k_{bank}) which is computed based on a best-fit to performance data. Large angles as $|\phi| \rightarrow 90^\circ$ would require special consideration and are not compatible with Eq. (11). The value of k_{bank} is defined to vary with flight segment for each aircraft.

The P_{ROCD} term was defined as given in Eq. (12).

$$P_{ROCD} = (ROCD - ROCD_0)\frac{m}{m_0}k_{ROCD,0}C_{ROCD} \quad (12)$$

Here, the nominally defined rate of climb or descent for a given flight segment is $ROCD_0$, the actual rate of climb or descent is $ROCD$, the actual mass as m and the reference mass as m_0 , $k_{ROCD,0}$ is a coefficient that varies with flight segment, and C_{ROCD} is a unit-conversion constant dependent on the units being used. Note that this P_{ROCD} increases linearly with m , consistent with the corresponding term in Eq. (4).

Finally, the P_{accel} term is defined as given in Eq. (13).

$$P_{accel} = m \left(k_{\dot{V}_{TAS,0}} \frac{V_{TAS}}{V_{TAS,0}} \right) \dot{V}_{TAS} + m \left(\frac{\rho_0}{\rho} k_{ROCD,0} + \frac{ROCD - ROCD_0}{C_{accel}} \right) ROCD \quad (13)$$

Subscript “0” indicates a reference condition obtained directly from the performance table model, ρ is the air density, and C_{accel} is a constant fit to the data for each aircraft. Note that Eq. (13) separates the acceleration in the horizontal (\dot{V}_{TAS}) and vertical ($ROCD$) directions, similar to the form of the TEM shown in Eq. (5).

Taken together, the performance tables and associated coefficients and equations provide a model that contains operations data including nominal flight profiles and segment definitions, detailed performance data in table form, and the capability of computing performance at arbitrary flight conditions. While BADA models fit parametric equations to available performance data to identify the performance (OPF) and procedures (APF) coefficients and then produce the performance tables (PTF and PTD) based on these coefficients, the approach taken in this work relies on a performance table to directly describe nominal operations and performance, and then introduces parametric equations to locally extend the model to nearby operating conditions. The motivation for utilizing this table-based modeling approach was that it allowed us to directly capture data at operating conditions of interest for vehicles with complex performance nonlinearities, while still adequately describing performance at arbitrary conditions not directly listed in the tables. In this sense, these table-based models can be viewed as a piecewise description of flight performance that provides precise performance data for conditions of greatest operational importance and offers parametric models to extend coverage to nearby areas of interest.

J. Applications of the Performance Model and Trajectory Simulation

Generally, performance models are not provided to users as a functional simulation. For the purposes of producing realistic trajectories complete with a time history of position, velocity, and fuel consumption, additional assumptions must be made, and a representative simulation must be constructed suitable to the user’s application. The required assumptions vary, but might include nominal acceleration limits, bank angle or turn rate limits, selection of flight planning algorithms, and intercept procedures for desired flight path, altitude, and airspeed. These details are usually not addressed in typical performance models (including BADA models), and thus were not part of the models developed in this work. Often, these decisions are based on the application and on an assessment of how the vehicle should be flown given the scenario under consideration. For example, in some applications flight maneuvers might need to be performed in a way to prioritize passenger comfort. In others, there may be a need to minimize the response time such as in a traffic deconfliction simulation. There are also applications in which transient details associated with maneuvering between flight segments can be safely ignored, and any transition between flight states can be assumed instantaneous. Thus, users are expected to carefully assess the needs of their application and then to apply the performance model in a manner that is consistent with these requirements.

A proof-of-concept dynamic MATLAB simulation was also developed to demonstrate the application of the performance models to computing realistic flight trajectories. This low-order dynamic simulation can provide detailed time histories of fuel burn or battery power consumption data and can be used to simulate envelope limitations due to power availability, such as might determine available acceleration or climb rate. The simulation incorporates both the basic performance table data as well as the provided parametric equations to model off-nominal conditions, banked turns, and accelerated flight. The successful implementation of the models in a simulation illustrated their practicality and allowed for comparisons of vehicle performance while flying similar missions.

An example of simulation output is shown in Fig. 12. This mission is not intended to represent a realistic UAM flight and is simply meant to demonstrate the basic functionality of the performance model and simulation. The mission begins from sea-level ISA conditions and consists of a vertical climb to 100 ft, a nominal climb to 2,000 ft, a nominal cruise for 37.5 nm, a nominal descent at cruise speed to 500 ft, transition to a “low-speed” descent to 100 ft, a deceleration to hover at 100 ft, and finally a vertical descent to the surface. Acceleration between segments is generally limited to 0.15 g’s and the power limitations of each aircraft are respected. From top to bottom, the plots on the left show power consumption, airspeed, and altitude. It can be observed that the Tiltwing completes the mission in the least time (about 23 min), followed by the Lift+Cruise (29 min), and the Quadrotor (31.5 min). This is unsurprising due to the mission length being driven primarily by the 37.5 nm cruise segment, which favors the much faster Tiltwing vehicle over the others. The right plot shows the power consumption in terms of percent fuel or battery

capacity consumed, with flight segments shown individually as a stacked bar graph for each aircraft. Each aircraft’s total power consumption is divided differently among the segments of flight. Specifically, the Quadrotor (“Quad”) uses more power in cruise than the other aircraft, while Lift+Cruise uses up more of its stored power in climb compared to the others. A detailed comparison of the relative performance of these vehicles is not the intention of this simulation or of Fig. 12. Nevertheless, the relative efficiency of each vehicle in certain segments of flight does lead to some fair conclusions about the strengths or weaknesses of certain designs. For example, the Quadrotor tends to be more efficient in slow flight and less efficient in cruise than the other aircraft, which is expected due to its reliance on rotor-based lift in all stages of flight.

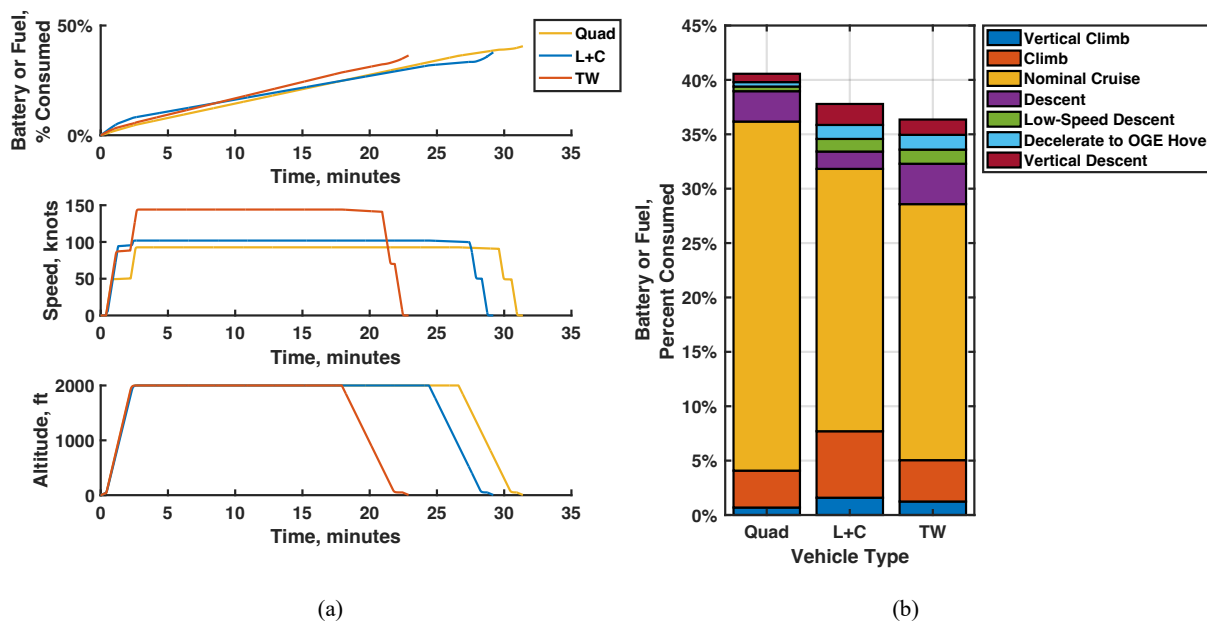


Fig. 12 Example of simulation results for the Quadrotor (Quad), Lift+Cruise (L+C), and Tiltwing (TW) vehicles, for a flight with a 37.5 nm cruise segment.

V. Conclusion

Performance modeling of UAM vehicles presents many challenges due to the absence of a fully defined operational environment, the limited availability of vehicle design details and performance data, and the lack of direct compatibility of existing modeling formats with UAM aircraft performance characteristics. This paper has discussed each of these issues and presented methods for developing performance models for the three representative UAM vehicles based on an analysis of NDARC-derived performance data. While this modeling effort succeeded in producing useful performance models, further development of appropriate model formats for UAM vehicles is needed, particularly as the vehicle designs mature and the operating environment becomes better defined. The development of a database for UAM performance models would also be beneficial to many stakeholders, and an effort toward developing an appropriate standardized interface to support this is discussed in Ref. [17]. Ideally such an interface standard would allow different types of models to be relatively interchangeable from the perspective of user applications, which could prove important as performance modeling methods for UAM vehicles evolve.

Future work will include a focus on more generalized UAM performance modeling methods, with increased attention to model parameterization, capture of performance-envelope limitations, development of optimization tools, and creating models with increased operational flexibility. Also important is the development of a better understanding of the complex aerodynamics present for many UAM vehicle designs. Accurate modeling of interaction effects between rotors, propellers, and aerodynamic surfaces and effectors is critical to designing these aircraft for reliable controllability and optimal efficiency, and performance models will need to accurately capture the performance impact of these characteristics. The successful growth of the UAM industry will depend on well-designed aircraft safely and efficiently integrating with ATM systems and regulations. Reliable performance models will serve an important role in the continued development of the broader UAM ecosystem, making continued progress in this area vital.

Acknowledgments

This work was funded by the NASA Air Traffic Management-eXploration (ATM-X) UAM Project. The authors would like to extend thanks to our colleagues in the NASA RVLT Project for providing the original NASA UAM vehicle designs and for their assistance with the NDARC software.

References

- [1] FAA NextGen Organization, "Urban Air Mobility (UAM) Concept of Operations (ConOps)," Technical Report, Federal Aviation Administration, 2020, URL: <https://arc.aiaa.org/doi/pdf/10.2514/6.2021-1626>.
- [2] Johnson, W., Silva, C., and Solis, E., "Concept Vehicles for VTOL Air Taxi Operations," AHS Technical Conference on Aeromechanics Design for Transformative Vertical Flight, January 2018.
- [3] Silva, C., Johnson, W. R., Solis, E., Patterson, M. D., and Antcliff, K. R., "VTOL Urban Air Mobility Concept Vehicles for Technology Development," AIAA 2018 Aviation Technology, Integration, and Operations Conference, AIAA AVIATION Forum, June 2018.
- [4] Whiteside, S. K. S., Pollard, B. P., Antcliff, K. R., Zawodny, N. S., Fei, X., Silva, C., and Medina, G. L., "Design of a Tiltwing Concept Vehicle for Urban Air Mobility," NASA TM-20210017971, June 2021.
- [5] Patterson, M. D., Antcliff, K. R., and Kohlman, L. W., "A Proposed Approach to Studying Urban Air Mobility Missions Including an Initial Exploration of Mission Requirements," AHS International 74th Annual Forum & Technology Display, 2018.
- [6] Johnson, W., "NDARC - NASA Design and Analysis of Rotorcraft," NASA TP-2015-218751, April 2015.
- [7] Antcliff, K., Whiteside, S., Kohlman, L. W., and Silva, C., "Baseline Assumptions and Future Research Areas for Urban Air Mobility Vehicles," AIAA SciTech 2019 Forum, January 2019.
- [8] Musialek, B., Munafo, C. F., Ryan, H., and Paglione, M., "Literature Survey of Trajectory Predictor Technology," U. S. Department of Transportation Federal Aviation Administration, William J. Hughes Technical Center DOT/FAA/TC-TN11/1, November 2010.
- [9] Peters, M., and Konyak, M. A., "The Engineering Analysis and Design of the Aircraft Dynamics Model for the FAA Target Generation Facility," Air Traffic Engineering Co., LLC, Prepared for The Federal Aviation Administration William J. Hughes Technical Center under FAA Prime Contract No. DTFAWA-10A-00020, October 2012.
- [10] Nuic, A., "User Manual for the Base of Aircraft Data (BADA) Revision 3.8," EUROCONTROL Experimental Center (EEC) Technical/Scientific Report No. 2010/003, April 2010, URL: <https://www.eurocontrol.int/publication/user-manual-base-aircraft-data-bada-revision-38>.
- [11] Nuic, A., Poles, D., and Mouillet, V., "BADA: An Advanced Aircraft Performance Model for Present and Future ATM Systems," International Journal of Adaptive Control and Signal Processing, Vol. 24, No. 10, 2010, pp. 850–866. <https://doi.org/10.1002/acs.1176>.
- [12] Mouillet, V., and Phu, D., "BADA Family H - A Simple Helicopter Performance Model for ATM Applications," IEEE/AIAA 37th Digital Avionics Systems Conference (DASC), 2018.
- [13] Sánchez, C. N., Sánchez, J. C., Ruiz, M. Á. V., Mouillet, V., and Nuić, A., "BADA EVTOL Performance Model for UTM Traffic Simulation and Analysis," 11th SESAR Innovation Days, December 2021.
- [14] Poles, D., "Base of aircraft data (BADA) aircraft performance modelling report," EUROCONTROL Experimental Center (EEC) Technical/Scientific Report No. 2009-009, March 2009.
- [15] Systems Analysis and Concepts Directorate, NASA Langley Research Center, Hampton VA., "NASA UAM Reference Vehicles," <https://sacd.larc.nasa.gov/uam-ref/>, Accessed Nov. 4, 2022.
- [16] Kadhiresan, A. R., and Duffy, M. J., "Conceptual Design and Mission Analysis for EVTOL Urban Air Mobility Flight Vehicle Configurations," AIAA Aviation 2019 Forum, Dallas, Texas, June 2019.
- [17] Hartman, D., Hartman, C., Foster, J., Morscheck F., Linke F., "An Interface Specification for Urban Air Mobility Performance Models to Support Air Traffic Management Research," AIAA SciTech 2023 Forum (submitted for publication), January 2023.